

Multipurpose x-ray reflectometer optimized for the characterization of organic surface films on aqueous subphases

P. Krüger and M. Schalke

Institute of Experimental Physics I, University of Leipzig, Linnéstr. 5, D-04103 Leipzig, Germany

J. Linderholm

JJ X-ray, CAT Science Park, Risø, DK-4000 Roskilde, Denmark

M. Lösche^{a)}

Institute of Experimental Physics I, University of Leipzig, Linnéstr. 5, D-04103 Leipzig, Germany

(Received 8 August 2000; accepted for publication 10 September 2000)

A reflectometer based on a conventional sealed x-ray source for the study of molecular organic surface films (such as Langmuir monolayers) has been devised, which outperforms similar instruments using rotating anode generators and approaches even most advanced experimental stations attached to third generation synchrotron sources. Reflectivities of $\sim 5 \times 10^{-9}$ are thus becoming available while the measurement of a full reflectivity curve takes approximately 4 h to complete. The instrument is operated under full digital control, permitting the automated recording of measurement programs. In an example of its performance we demonstrate that dipalmitoylphosphatidylglycerol monolayers on electrolytic subphases may be characterized to a level of detail which until recently was not even available at synchrotron sources. While conventional box models of lipid monolayers are inadequate for modeling experimental data at the high momentum transfer that has become accessible with the new instrument, a recently developed modeling technique based on volume-restricted distribution functions [Schalke *et al.*, *Biochim. Biophys. Acta* **1464**, 113 (2000)] enables studies of ion binding to the phospholipid in submolecular detail. © 2001 American Institute of Physics. [DOI: 10.1063/1.1331329]

I. INTRODUCTION

Molecular organic films on aqueous surfaces and at solid/fluid interfaces show complex supramolecular organization forms that may be characterized with a variety of surface sensitive methods developed in the past two decades. While laser-optical techniques such as fluorescence^{1–3} and Brewster angle microscopy,^{4,5} ellipsometry⁶ and ellipsometric microscopy,⁷ or surface-plasmon spectroscopy⁸ are sensitive to monomolecular surface films, they report their optical properties, such as the index of refraction or the layer thickness, at best semiquantitatively.⁷ They are, however, methods very well capable of characterizing the lateral organization of such surface films on the mesoscopic length scale. Raman^{9,10} and Fourier transform spectroscopy in the reflection-absorption mode^{11,12} are well-established techniques to probe molecular interactions within organic surface films. This has been exploited to investigate the order in aliphatic lipid chains empirically, to characterize hydrogen bonding in molecular films,¹³ and to determine the orientation of transition dipole moments with respect to the interface.¹²

Surface sensitive x-ray and neutron scattering, i.e., x-ray diffraction at grazing incidence (GIXD), and x-ray as well as neutron reflectometry, have been extensively used to deter-

mine the structure of organic surface or interface films in molecular detail.^{14–16} While GIXD is capable of assessing the molecular order of hexatic or crystalline surface films, such as lipid monolayers^{17,18} or protein sheet crystals,^{19–21} specular reflectometry using x rays or neutrons determines the scattering length density (SLD) profiles, i.e., electron density or neutron SLD, normal to the interface.^{14,22,23} Both types of x-ray experiments have been developed using the extremely brilliant and well-collimated x-ray beams only available at synchrotron radiation facilities.¹⁵ More recently, however, x-ray reflectometry of floating surface monolayers has been brought to the laboratory scale, where measurements down to the level of $R \sim 10^{-7}$ have been routinely achieved.^{24,25}

We report here the design of a new x-ray reflectometer for the investigation of molecular organic films on fluid surfaces. It is based on a conventional sealed-tube source in connection with a multilayered parabolic monochromator mirror and a detection scheme that enables the simultaneous determination of signal and background using a position-sensitive detector (PSD). This instrumentation is so sensitive as to measure reflectivities down to $R \sim 5 \times 10^{-9}$ within data acquisition times of typically 4 h, a performance that has until recently only been available at synchrotron radiation sources.

Chemical models used for the interpretation of reflectivity data from lipid surface monolayers have been frequently composed of a hydrophobic slab of aliphatic chains and a

^{a)}Author to whom correspondence should be addressed; electronic mail: loesche@physik.uni-leipzig.de

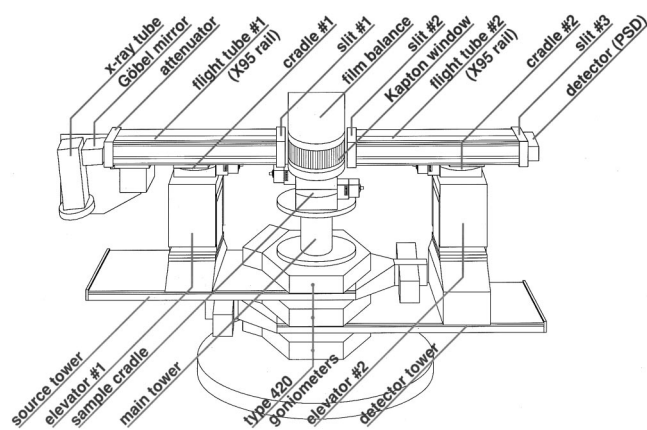


FIG. 1. Schematic viewgraph of the multipurpose x-ray reflectometer.

hydrophilic slab of hydrated headgroups. In such models, the interfaces between the bulk subphase, the 2 monolayer slabs, and the gas compartment are blurred by one surface roughness parameter σ that accounts for thermally excited capillary waves which are thought to affect the electron density gradients identically at all interfaces.^{15,26} This is equivalent to conceiving the hydrophilic/hydrophobic interface within a monolayer as infinitely sharp. With such models, reflectivity data of lipid monolayers up to $q_z^{\max} \sim 0.5 \text{ \AA}^{-1}$ (where q_z is the momentum transfer which is in specular reflectivity experiments collinear with the surface normal z) have been successfully described²⁷ and the results have been checked for consistency by comparing the integrated scattering length, i.e., the number of electrons contained in the hydrophobic slab per unit area, with the molecular density at the interface as retrieved from isotherms. The molecular composition of the hydrophilic slab follows then from the scattering length per unit area in that slab in that electrons in excess of the number expected for the lipid headgroup, as derived from the lateral molecular density in the film, are attributed to interpenetrating water molecules.^{23,28}

With third generation synchrotron sources becoming available²⁹ and—as we show here—with the development of highly efficient laboratory scale x-ray reflectometers, it has been possible to push the limits of resolution (with $q_z^{\max} \sim 1.0$ and 0.75 \AA^{-1} for synchrotron and conventional sources, respectively).²⁸ This enables us to check the assumptions that have been made in the interpretation of the more limited data sets.

II. INSTRUMENTATION AND EXPERIMENTAL DETAILS

A. X-ray reflectometer

The core of the butterfly-type reflectometer—devised to measure small-angle scattering from a horizontal sample surface—consists of three uniaxially aligned goniometers (Model No. 420, Huber, Garching, Germany) carrying the sample stage, the x-ray tube, and detector pivot towers, cf. Fig. 1. The sample may consist of either a fluid surface, contained within the sealed sample compartment of a Langmuir film balance, or a planar solid surface. The sample stage allows elevation (type II elevator, JJ X ray), tilting, and

translation (Huber goniometer head, part No. 5203.2, and x - y stage, part No. 5102.2). Both detector and tube towers incorporate an elevator (type I elevator, JJ X ray) and a cradle (Huber, part No. 5202.4). The cradles shoulder 500 mm long Newport X95 rails whose cores are sealed with Kapton windows and serve as evacuated flight tubes for the x-ray beam. Except for the entrance window of the first rail, which carries Cu absorbers to optionally attenuate the incident beam, the flight tubes are terminated at both ends by adjustable pairs of horizontal and vertical slits.

The x-ray beam is conditioned, controlled, and detected as follows. The white beam from a conventional sealed x-ray tube with Cu target, typically operated at 1575 W (45 kV/35 mA) at a stabilized temperature of $T \sim 40^\circ \text{C}$ (type S tube housing with Kristalloflex 760 power supply, Bruker AXS, Karlsruhe, Germany) feeds a graded W/Si multilayer mirror (“Göbel mirror,” AXS) matched to the $\text{Cu } K_{\alpha 1}$ line at $\lambda \sim 1.541 \text{ \AA}$, where its throughput ($\sim 80\%$) is at least 3 orders of magnitude larger than that for the $\text{Cu } K_{\beta}$ line. The well-collimated and monochromated output from this device is the source of the reflectometer. The parallel beam is $\sim 600 \mu\text{m}$ in height and $\sim 8 \text{ mm}$ in width. Its flux at 1575 W input power is typically 4.5×10^7 photon/s. Monitoring of the primary intensity may be compromised because of the high stability of the power supply after an appropriate period (typically 2–3 h) for temperature stabilization after a cold start.

The mechanical setup, as sketched above, allows control of the incident angle α_i in the range $0^\circ \sim 7^\circ$, and determination of the intensity reflected from the sample at the specular position α_f . Immediately after the Göbel mirror, the impinging beam passes a set of calibrated Cu attenuators used either individually or in combinations³⁰ to reduce the primary beam intensity to a level such that the reflected intensity falls into the linear regime of the detector response ($< 2000 \text{ counts s}^{-1}$). After the first flight tube the beam passes an entrance slit that controls the beam height to avoid beam footprints in the sample plane that are larger than the sample area. After reflection from the sample, the x-ray beam is received in a slit/flight tube/slit combination for discrimination against incoherently scattered photons from the subphase. The reflected intensity is measured with a horizontally aligned position-sensitive gas detector (Ar/methane at 7 bar, PSD-50, M. Braun, Munich, Germany). For reflectivity measurements at liquid surfaces, precise determination of both signal and background is mandatory. Particularly at low reflectivities, long counting times are required to achieve good counting statistics. The PSD permits simultaneous signal and background determination by measuring the two quantities in different parts of its sensitive area while the detector arm is rotated out of the plane defined by the incident beam and the surface normal by $\sim 2^\circ$. This not only reduces data acquisition time by a factor of 2, but also helps avoid systematic errors that may occur by repeated shuttling of the detector between the specular and off-specular positions for alternating signal and background determination.

The detector signals are evaluated using an analog to digital converter (Canberra model No. 8701) which stores its results in a histogramming memory (Risø National Labora-

tory, Denmark). All components are driven by stepper motors using an ECB module (Risø) as interface to the control computer.

Primarily, the machine is designed as a Θ - Θ (butterfly type) diffractometer for reflectometry of horizontal samples and fluid surfaces. Due to the large number of controlled mechanical degrees of freedom and the high photon flux, however, it may also be readily used as a small x-ray and wide angle diffractometer after a few setup changes. Transformation back to reflectivity mode requires only minor realignment.

B. Sample environment

Most investigations of the machine described here concern reflectometry studies of Langmuir monolayers at the air/water interface. Such surface films are prepared in a Langmuir trough of local design (subphase volume, $160 \times 300 \times 5.5 \text{ mm}^3$) which is similar to the one we have devised earlier for use at BW1 (DESY, Hamburg).³¹ Both trough and barrier are made from Teflon polytetrafluoroethylene (PTFE). The smallest area to which the film may be compressed by means of a motorized barrier is $\sim 75 \times 160 \text{ mm}^2$. The subphase temperature is controlled using an immersed TFE-coated Pt-100 sensor whose signal is fed back to the power supply of 20 Peltier elements distributed underneath the trough bottom ($P_{\text{max}} \sim 250 \text{ W}$). To suppress surface waves underneath the beam footprint, a polished glass block ($160 \times 60 \times 5 \text{ mm}^3$) may be inserted into the subphase to reduce the subphase depth locally to below $500 \mu\text{m}$. This option is only necessary for measurements at bare water surfaces or with films of low pressure. The surface pressure of the film, $\pi = \gamma_0 - \gamma$ (where γ and γ_0 are the surface tensions of the film covered and the clean water subphase), is measured using a Wilhelmy balance operated with ash-free filter paper. The film balance is contained within a gas-tight container sealed with a Kapton window (thickness, $80 \mu\text{m}$, Goodfellow, Bad Nauheim, Germany) that allows the incident and reflected beams to enter from or into the flight tubes, respectively. The whole box is mounted on a Huber 5102.2 x - y stage on top of a 5203.2 goniometer head (cf. Fig. 1).

C. Master computer and wiring; operation modes

The entire machine is controlled by a Linux work station via a user modified TASCOS package (Risø). The main communication wire is a general purpose interface bus (GPIB) chain that connects all devices. Small devices—Langmuir balance and temperature controller—are attached to the main chain via a quadruple GPIB/RS232 converter (Fig. 2). The homebuilt Langmuir film balance controller is readable and instructible. It drives the film balance mechanics and operates the Wilhelmy sensor. Its operation modes include maintaining a constant surface pressure or constant area, compressing/expanding the monolayer at a user-defined barrier speed, or driving the barrier continuously back or forth for cleansing.

Owing to the full digital control over all components of the machine, measurement sequences on a single sample at

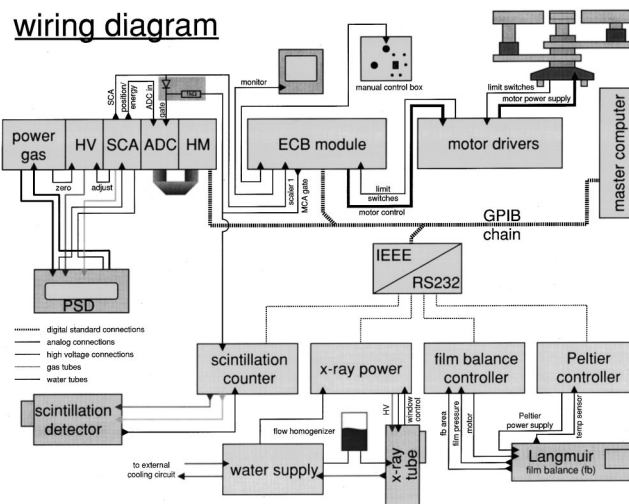


FIG. 2. Wiring diagram of the instrument.

different preparation conditions may be executed. For Langmuir monolayers, reflectivity measurements as a function of surface pressure π at constant temperature T or as a function of T at constant π are often intended. Another option is the tracing of (slow) time-dependent processes. A typical measurement task is divided in two sections: preparation of the requested state of the sample (control program) and sample characterization (main routine). Both tasks may be repeated to perform complex series of measurements. Typically, the control program starts barrier compression and stops it as the desired lateral pressure has been reached. Afterward it may wait for an appropriate time span to allow for equilibration of the sample film. Subsequently, the main measurement routine takes over control and performs several tasks: control of the motors and readout of the PSD; realignment to compensate for water level changes; control of the attenuator to optimize counting statistics and protect the detector; control of the beam size by adjusting the slits to avoid oversized beam footprints on the one hand and to utilize a maximum of the x-ray intensity on the other; optimization of the count time depending on the actual reflectivity at a given momentum transfer; adjustment of the step width of the sampled momentum transfer values depending on the local slope of the reflectivity curve; and data processing and storage.

D. Reflectivity measurements

On water, reflectivities down to 5×10^{-9} are routinely achieved within $\sim 4 \text{ h}$ measurement time with a sufficient density of data points. For typical lipid surface films, such values of the reflectivity are reached at angles $\alpha_i \leq 5^\circ$ and may be accessed using the motion range of the detector and tube towers exclusively—keeping the sample film at a constant position. This is important for the investigation of vibration sensitive samples such as two-dimensional protein crystals at water surfaces.²⁰ For $\alpha_i > 5.2^\circ$, the sample itself must be moved vertically until at $\alpha_i \sim 7^\circ$ the mechanical limits of the cradles are reached.

Alternatively, for the tracking of slow dynamical processes, reflectivity curves limited to a more confined momentum transfer range between 0 and 0.5 \AA^{-1} ($\alpha_i \sim 3.5^\circ$) are

obtained within 1 h and may represent a snapshot of the sample structure. Faster dynamics of structural reorganizations may be captured by adjusting the instrument to a fixed momentum transfer, preferably at a position where the final surface film is characterized by an interference minimum, and measuring continuously the reflectivity at this q_z value.

In standard measurements of reflectivity curves of molecular surface films, the height of the impinging beam is changed at $\alpha_i = 0.7^\circ$ from $100 \mu\text{m}$ —appropriate to measure the total reflection regime between 0.1° and 0.15° —to the full beam cross section of $600 \mu\text{m}$. Due to an approximately Gaussian profile of the raw beam this results in an intensity gain of a factor of ~ 5 . The precise scaling factors have been determined prior to the experiment.

Using the attenuator, the count rate in the detector, integrated over its entire length, is kept in the range between 600 and 1500 s^{-1} as long as possible (at high momentum transfer, count rates dwindle as the reflectivity dips down). The step width for sampling the reflectivity curves is currently adjusted according to the intensity of the reflected beam, in essence by concurrently doubling the step width and the maximum dwell time as the count rate falls below a preset threshold. The maximum step width used is 0.2° and the dwell time is limited to 1000 s.

Beam damage as it happens in reflectivity or GIXD measurements on organic surface monolayers at synchrotron sources was never observed. Third generation synchrotron sources^{19,20} (e.g., BW1 at HASYLAB, Hamburg, Germany) deliver typically 10^{12} photons/s at the sample. This implies that 1 s of full synchrotron beam is equivalent to more than 4 h of illumination in the full beam of the home-based device. This comparison illustrates why beam damage is not a concern in the instrument described here.

E. Chemicals

Spreading solutions of *L*- α -dipalmitoylphosphatidyl-rac-glycerol (DPPG) (Sigma-Aldrich, Deisenhofen, Germany) were prepared in chloroform/methanol (4:1 v:v) (p.a. grade, Merck, Darmstadt, Germany) with concentrations of $\sim 0.3 \text{ g/l}$. BaCl_2 (p.a. grade) was from Sigma-Aldrich. Ultrapure water (Millipore Milli-Q RG, Eschborn, Germany, resistivity $>18.2 \text{ M}\Omega \text{ cm}$) was used for the subphases.

III. EXEMPLARY RESULTS AND RESOLUTION

A typical reflectivity curve R versus momentum transfer $q_z = (4\pi/\lambda)\sin\alpha_i$, for a DPPG monolayer on 10 mM BaCl_2 at $\pi = 30 \text{ mN/m}$ and $T \sim 20^\circ \text{C}$ measured on the instrument described here is shown in Fig. 3 (full symbols) and compared with a synchrotron data set obtained under the same nominal conditions (open symbols). Experimental error bars are shown on all data points and are in most cases smaller than the print symbols. Remarkably, the lower limit of the reflectivity data that may be discriminated against the experimental background³² at the synchrotron experimental station ($R \geq 10^{-10}$) is only 1.5 orders of magnitude below the one at the laboratory based x-ray source ($R \geq 5 \times 10^{-9}$). Above the critical angle α_c for total reflection, the reflectivity curves follow the Fresnel reflectivity R_F modulated by interference

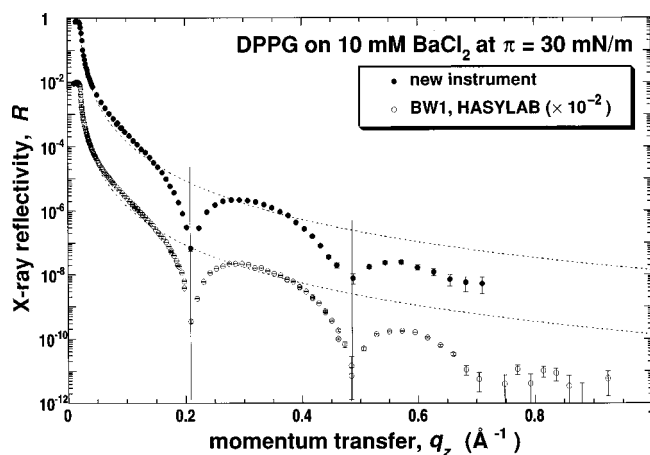


FIG. 3. X-ray reflectograms, reflectivity R vs momentum transfer q_z , of DPPG monolayers on 10 mM BaCl_2 at $\pi = 30 \text{ mN/m}$, $T = 20^\circ \text{C}$ measured on the newly designed home-based instrument (upper data set) and at the undulator beamline BW1 of HASYLAB (DESY, Hamburg). In most cases, the experimental error bars, determined from counting statistics, are smaller than the print symbols. The BW1 data have been offset by a factor of 10^{-2} for clarity. Dashed curves show the Fresnel reflectivity. Vertical lines indicate the interference minima in the data.

that depends on the structure of the surface monolayer. For water with $\rho_e \sim 0.3336 \text{ e}^-/\text{\AA}^3$ and $\lambda \sim 1.541 \text{ \AA}$, the critical angle is $\alpha_c \sim 0.15^\circ$.

Figure 4 shows Fresnel-normalized reflectivity data R/R_F of DPPG on an aqueous subphase with 10 mM BaCl_2 at $T \sim 20^\circ \text{C}$ at various surface pressures between $\pi = 20$ and 45 mN/m collected in one run on a single monolayer that lasted $\sim 24 \text{ h}$. For six reflectivity curves at the BW1 facility, one needs at least two preparations and roughly 12 h of continuous beamtime. The data have been normalized by the Fresnel reflectivity of the pure subphase in order to emphasize the modulation of the reflectivity inferred by the pres-

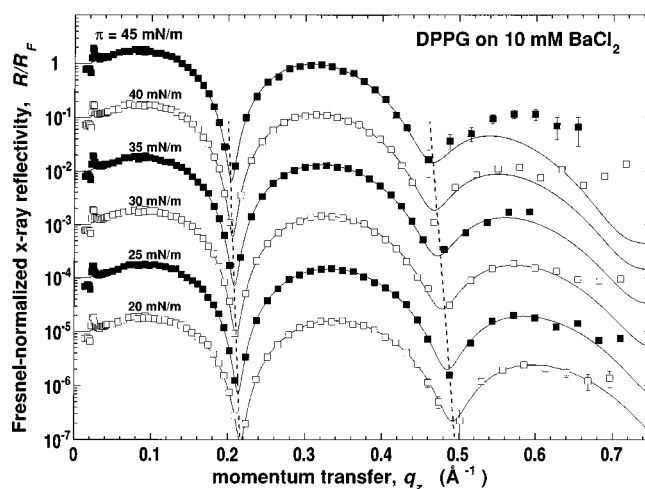


FIG. 4. Series of Fresnel-normalized x-ray reflectograms, reflectivity R/R_F vs momentum transfer q_z measured for a DPPG monolayer on 10 mM BaCl_2 at various lateral pressure values as indicated. $T = 20^\circ \text{C}$. Experimental error bars are only given for the data at the lowest and highest pressure. The reflectivity scale applies to the data at $\pi = 45 \text{ mN/m}$. For clarity, data sets are offset by factors of 10 for lower pressures. Straight dashed lines connect the interference minima in the data to indicate how the monolayer thickness increases upon compression. Continuous curves indicate the x-ray reflectivities derived from the VRDF model (see the text).

ence of the molecular surface film. The data set at $\pi = 30$ mN/m is the same as the one shown in Fig. 3 with full symbols. All data sets show two pronounced minima which are due to destructive interference between amplitudes reflected off the surface of the lipid monolayer toward the gas compartment and the interface where the monolayer is in contact with the aqueous subphase. These minima are thus characteristic of the thickness of the lipid monolayer film. As the film is compressed, the positions of the minima shift to smaller q_z values, indicative of an increase of the monolayer thickness. Quantitatively, by evaluating the layer thickness as

$$d_{\text{ml}} = \frac{2\pi}{\Delta q_{z,\text{min}}}, \quad (1)$$

one observes an increase from $d_{\text{ml}} \sim 23 \text{ \AA}$ at $\pi = 20$ mN/m to $d_{\text{ml}} \sim 25 \text{ \AA}$ at 45 mN/m. Similar observations have been reported for many amphiphilic monolayers in the literature.^{25–27,33}

Further details on the conformation of the film-forming molecules are contained in the line shape of the reflectivity curves. As in other scattering techniques, the intrinsic resolution of a reflectivity experiment is determined by the sampling theorem

$$\Delta z \approx \frac{\pi}{q_z^{\text{max}}} \quad (2)$$

(where q_z^{max} is the maximum of the experimentally accessible momentum transfer) if there is no other information on the sample structure available. Typical values of q_z^{max} in experiments that marked until recently the state-of-the-art for x-ray reflectivity measurements of film structures on aqueous subphases were around 0.4 \AA^{-1} , both in measurements using synchrotron and conventional x-ray sources, corresponding to an intrinsic resolution of $\Delta z \sim 8 \text{ \AA}$. The new instrument described here pushes the limits of resolution quite considerably: The data presented in Fig. 3 extend up to $q_z \sim 0.7 \text{ \AA}^{-1}$, equivalent to $\Delta z \sim 4.5 \text{ \AA}$.

IV. DATA INVERSION AND DISCUSSION

As extensively discussed in the literature,^{14–16} $R(q_z)$ is approximately connected with $\rho_e(z)$ by

$$\frac{R(q_z)}{R_F(q_z)} = \left| \frac{1}{\rho_e^{\text{subphase}}} \int \frac{d\rho_e(z)}{dz} \exp(-iq_z z) dz \right|^2, \quad (3)$$

where z is the distance from the interface. Due to the lack of phase information, R cannot directly be inverted to obtain $\rho_e(z)$. Rather, the optical parameters are refined by least-square fitting of model reflectivities to the experimental data. The simplest approach is using layer models (“box models”),²⁶ motivated by the propensity of amphiphilic molecules for supramolecular self-organization into molecular surface films. A collective roughening of the interface structure by thermally excited capillary waves^{34,35} is usually accounted for by convoluting the layer structure with a Gaussian function characterized by a width parameter σ . Alternatively, model-free techniques to data inversion have been developed.^{36–40} Beyond the chemically motivated layer

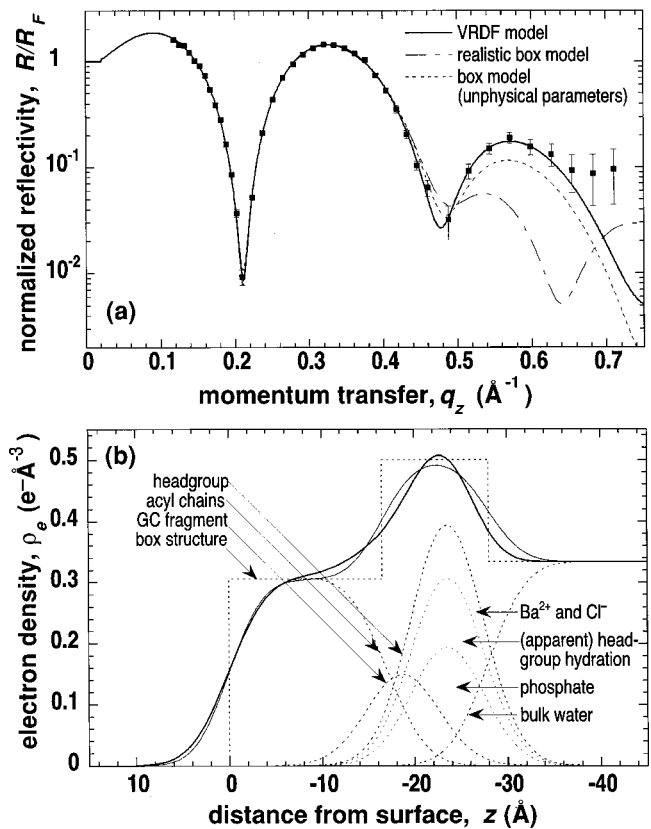


FIG. 5. Data modeling using various approaches. (a) Reflectivities of best-fit models of the DPPG/BaCl₂ data set at $\pi = 30$ mN/m derived using the VRDF approach (continuous line), a physically sensible box approach (two slabs, one surface roughness parameter σ ; dash-dotted line), and a box model approach with unphysical parameters (two slabs, three surface roughness parameters σ_i ; $\rho_e^{\text{headgroup}} > 0.75 \text{ e}^-/\text{\AA}^3$ and large σ_0, σ_1 ; dotted line). Two-box models generally fail to describe the reflectivity data satisfactorily beyond $q_z \sim 0.5 \text{ \AA}^{-1}$. Best-fit three-box models with distinct surface roughness parameters σ_i or model-free data inversion techniques (Ref. 36) were found to yield solutions whose electron densities were similar to that of the VRDF model. (b) Structural differences of the electron density profiles obtained with the conventional slab models and the VRDF model. Shown are profiles that describe the data set taken at $\pi = 30$ mN/m best in the frame of a two-box model with one global surface roughness (thin continuous line) or the VRDF approach (thick line). Sensible electron density profiles derived from the model-free approach were virtually indistinguishable from that of the VRDF model. Dashed lines indicate the box structure as it would appear without surface roughness and the components of the VRDF model.

models, we have developed a composition-space refinement^{23,41} method that uses volumetric information derived from molecular modeling by Feller and co-workers.^{42,43} It describes the structure of a lipid monolayer as a volume-restricted sum of distribution functions (VRDFs) of lipid molecule fragments across the interface and follows the general line of the data inversion procedure described for the interpretation of small-angle diffraction from lipid multibilayer stacks;^{43,44} it has been described in detail elsewhere.^{28,45}

With conventional two-slab models we have not been able to describe satisfactorily the experimental data shown in Fig. 4. While such models perform well in the q_z regime covering the first two maxima of R/R_F , they are often found incapable of modeling the data beyond $q_z = 0.5 \text{ \AA}^{-1}$, cf. Fig. 5(a). This is also true if one uses surface roughness parameters σ_i ($i = 0, 1, 2$ for the subphase/headgroup, headgroup/

chain, and chain/air interfaces, respectively) that may differ for the distinct interfaces of the two slabs. Only upon extending the two-slab model into a three-slab model with distinct σ_i ($i=0,\dots,3$) were we able to describe the experimental data satisfactorily. However, at the same time we found that various parameter sets which result in similar $\rho_e(z)$ describe the reflectivity data equally well. That is, the electron density profile of the monolayer is overdetermined by a three-slab model. While the profiles resulting from the various distinct solutions after convolution with the surface roughness functions are indistinguishable, their parenting box structures, i.e., the profiles *without* surface roughness, are quite different. Consequently, most or all of such “best-fit” parameter sets are physically irrelevant; moreover, they do not lend themselves to a molecular interpretation.

The major justification for the application of layer models in the description of surface monolayers has been their apparent natural faculty for a molecular interpretation of such systems. In view of the failure of genuine two-layer models to describe data sets at large q_z and in view of the inaccessibility of more complex layer models for a molecular interpretation, one may as well resort to model-free data inversion methods, which are generally not intended for an interpretation of the surface structure in molecular terms. We have used the approach developed by Skov Pedersen and Hamley,^{36,37} which uses *B*-spline functions to parameterize the electron density profile across the interface. The resulting electron density profiles are virtually indistinguishable from the profiles derived from the complex layer models. This suggests that the surface film may indeed be described by a *unique* electron density profile, which can be deduced irrespective of the method used for inversion of the extended data sets.

Compared to electron density profiles derived from two-slab models based on more restricted data sets, the high-resolution profiles are particularly distinctive in the hydrophilic headgroup region. For the data set that corresponds to the DPPG monolayer at $\pi=30$ mN/m, Fig. 5(a) compares the best-fit electron density profiles derived from the genuine two-box model and the free-form fitting. This comparison reveals that the transition in electron density from the hydrophobic chain region ($\rho_e \sim 0.3 e^-/\text{\AA}^3$ at $z > -15$ \AA) to the region where the profile attains its maximum ($\rho_e \sim 0.48 e^-/\text{\AA}^3$) due to the electron-rich phosphates within the lipid headgroups is more structured than the established two-slab model would suggest. This finding implies that structural features of the headgroups, which are not accessible in the low-resolution data, may be assessed at higher resolution. Trying to unveil the available information motivated the development of the VRDF method, a new and general modeling strategy for data inversion in reflectivity measurements of lipid layers.^{28,45,46} In brief, distribution functions are used to describe the arrangement of functional molecular fragments of the film-forming amphiphiles across the interface. Volumetric information obtained from molecular dynamics simulations of bilayer systems^{42,43} are utilized to constrain the models. Thus, phospholipid molecules are parsed into various fragments which contain their acyl chains (ACs), glycerol and carbonyl moieties (GCs), the phosphate

(P), and the remainder (*R*) of the headgroup. The AC fragment is treated similarly as in the conventional box models. For the remaining fragments, Gaussian distribution functions are used. *R* is empty for phosphatidic acids or contains the cholin, ethanolamine, or (secondary) glycerol moieties for various other phospholipid species. In terms of their electron densities, the fragments described by *R* are often similar to water and thus inaccessible in x-ray reflection measurements. Neutron reflectivity, particularly on deuterated compounds such as headgroup-labeled DPPC-d₉, is hoped to afford a detailed assessment of this part of lipid headgroup structure.

To keep the number of independent parameters low, the GC fragment has been strictly coupled to the AC fragment.⁴⁵ For the DPPG data analyzed in this work, the secondary glycerol, whose electron density is essentially that of water, has not been explicitly accounted for. Consequently, scattering length dubbed “water” in the headgroup—or subphase water immediate underneath the headgroup—contains the electrons located on this fragment. On the other hand, the VRDF model included explicitly both Ba^{2+} and Cl^- ions that were presumed to be bound to the PG headgroup. As with DMPA monolayers,²⁸ we observed that significantly more than 0.5 Ba^{2+} ions were predicted to be bound per PG headgroup by a model that did not allow for the simultaneous binding of Cl^- anions and Ba^{2+} cations. This would have resulted in a charge reversal in the lipid headgroup layer to a net positive area density of electric charges—a rather unlikely scenario. A more reasonable interpretation of the experimentally observed high electron density in the headgroup is to assume that both Ba^{2+} and Cl^- are bound in different concentrations. Since the introduction of headgroup-bound Cl^- , formally treated as the binding of a BaCl^+ cation, brought about one extra model parameter (both BaCl^+ and Ba^{2+} were assumed to be located at the same distance from the interface as the center of the P fragment), the model assumed an electroneutral headgroup layer.⁴⁷ Water molecules introduced into the headgroup by either the Ba^{2+} or BaCl^+ cation are indistinguishable from the hydration shell of the phosphate itself. Using this model, we have been able to describe the data shown in Fig. 4 satisfactorily and consistently, as indicated by the lines included in Fig. 4 and as shown in Fig. 6.

Figure 6 indicates the development of the best fit parameters as a function of lateral pressure π . The molecular area values determined from the isotherm, which is included in Fig. 6(a) for reference, have been used as constants in the fitting procedure. As reported earlier for DMPA monolayers,^{28,45} the collective surface roughness σ_{CW} , attributed to thermally excited capillary waves at the surface, increases with π and develops as expected^{34,35} (data not shown). Quantitatively, the values for σ_{CW} measured here vary continuously between 2.95 \AA at 20 mN/m and 3.95 \AA at 45 mN/m and lie thus within ± 0.1 \AA of those values observed at similar pressures for the DMPA system.

The hydrophobic chain slab thickness increases linearly upon compression—from $d_{\text{AC}} \sim 16.4 \pm 0.3$ \AA at $\pi=20$ mN/m to $\sim 18.1 \pm 0.8$ \AA at 45 mN/m—within the regime of low compressibility of the isotherm [see Fig. 6(a)]. The fact that the molecular area of DPPG, as observed in the isotherm, is

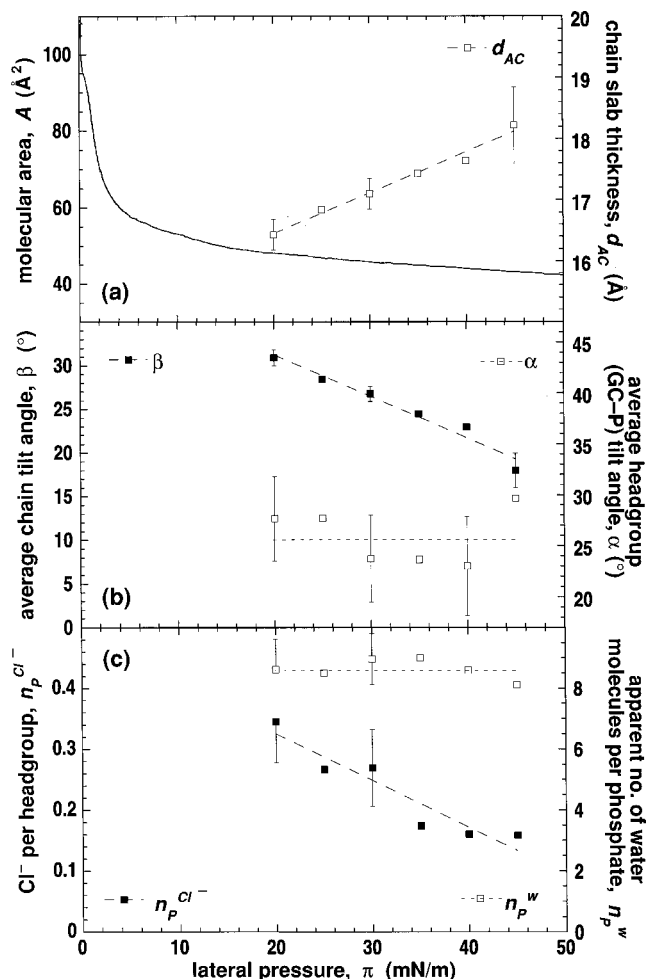


FIG. 6. Best-fit parameters (VRDF model) describing the structure of a DPPG monolayer on 10 mM BaCl₂ as a function of surface pressure π . (a) Isotherm as measured with the Wilhelmy balance (left scale, continuous line) and average hydrocarbon slab thickness d_{AC} . (b) Average chain tilt angle $\beta = \arccos(d_{AC}/l_{chain})$, where $l_{chain} = 19.15 \text{ \AA}$ is the extended length of a palmitoyl chain (Ref. 23) (left) and average headgroup tilt angle $\alpha = \arccos(d_{GC-P}/l_{GC-P})$, where $l_{GC-P} = 5.27 \text{ \AA}$ (see Ref. 45). (c) Number of Cl⁻ anions, $n_p^{Cl^-}$ (left) and of water molecules n_p^w bound per phosphate in the lipid headgroup. The scattering lengths attributed to water may also contain contributions from the secondary glycerol within the PG headgroup that is likely to partially intercalate the phosphate moieties. The total number of bound Ba²⁺ cations is $1/2(1 + n_p^{BaCl^-})$ in the simplified VRDF model (see the text). Dashed lines are guides for the eye.

20% (at 20 mN/m) to 10% (at 45 mN/m) larger than the limiting area for two acyl chains, $A_0 \sim 40 \text{ \AA}^2$, as determined from GIXD,⁴⁸ is consistent with the observation that the chain slab thickness never attains a value corresponding to the length of a fully extended acyl chain ($l_{chain} = 19.15 \text{ \AA}$, cf. Ref. 23). The average acyl chain inclination angles against the surface normal β are thus significantly larger than zero at all lateral pressures. As shown in Fig. 6(b) (left), β varies between 31° and 18°; these values are thus intermediate between those measured for DPPC ($\beta \sim 30^\circ$ at 42 mN/m²³) and DMPA ($\beta \sim 15^\circ$ at π values between 30 and 50 mN/m^{28,45}) in monolayers at high pressure.

As shown in previous work,²⁸ the VRDF model may reveal genuinely new information particularly on lipid headgroups, while the assessment of hydrocarbon chain structure

yields results similar to those obtained from box models. In the following, we focus thus on the PG moieties with ions bound from the subphase. In evaluating the lipid headgroup structure, the partial volumes of the GC and P moieties have been assumed to be $V_{GC} = 146.8 \text{ \AA}^3$ and $V_P = 53.7 \text{ \AA}^3$, respectively,⁴³ and the GC fragment has been immediately coupled to the acyl chains in the model.⁴⁵ A determination of the centers of gravity of the GC and P moieties, together with an estimate of the maximum distance between GC and P ($l_{GC-P} \sim 5.3 \text{ \AA}$, cf. Ref. 45), enables a measurement of the average inclination angle α of the GC→P orientation within the headgroups [see Fig. 6(b) (right)]. As observed for DMPA on ionic subphases,²⁸ α is essentially constant along the isotherm, despite a continuous decrease in area per molecule and a corresponding straightening of the chains as indicated in Fig. 6(b) (left). In distinction to the results obtained for DMPA monolayers, the GC→P orientation is closer to the surface normal, $\alpha \sim 25^\circ \pm 8^\circ$ for DPPG on BaCl₂ versus $\sim 45^\circ$ or $\sim 37^\circ$ for DMPA on water or BaCl₂, respectively. This is clear indication that the secondary glycerols partially intercalate the phosphates in the headgroup slab, presumably forming hydrogen bonds between the C–OH and the P=O groups. Consistent with this conjecture, we observe scattering length, formally attributed to phosphate-bound water [$n_p^w = 8.5 \pm 1$, see Fig. 6(c)] that is consistently above the value reported for DMPA under similar conditions ($n_p^w = 5.5 \pm 1$).²⁸ We suggest that phosphate hydration in PG, as revealed from the x-ray reflectivity measurements, is thus an *apparent* quantity which includes scattering length of the secondary glycerol. Since a glycerol moiety contributes to the electron density roughly the same number of electrons and the same volume as do three water molecules, it is tempting to speculate that the hydration of the phosphate moieties in PG and PA are quite similar and that the differences in headgroup structure are mainly due to the secondary glycerol, which may have its center of mass located at a similar distance from the interface as the phosphate. The observation that the large apparent hydration is constant as a function of pressure suggests that glycerol intercalation into the phosphate region does not significantly change upon compression.

Why doesn't the lipid headgroup change its conformation while the area per molecule decreases by 20% along the isotherm and the acyl chain orientation changes accordingly? As with DMPA monolayers on BaCl₂,²⁸ we observe that Cl⁻ anions are bound together with Ba²⁺ cations in significant amounts and are continuously expelled from the headgroup upon compression of the monolayer [cf. Fig. 6(c)]. This conclusion derives from the fact that significantly more electrons are needed in the lipid headgroup to model the experimental results than those supplied by one phosphatidylglycerol moiety plus 0.5 of a Ba²⁺ cation (which would be the headgroup composition if one assumes stoichiometric binding of subphase cations to lipid headgroup anions). Since it is quite unlikely that *more* Ba²⁺ is bound than needed for charge neutralization of the headgroup, which would lead to an overcompensation of charges, we prefer the alternate interpretation that Ba²⁺ and Cl⁻ is concomitantly bound. Since a quantification of such a model would require an independent

cdetermination of both cation and anion concentration in the headgroup, e.g., in a contrast variation measurement that is not available at this time (see *Note Added in Proof*), we determine Ba^{2+} and Cl^- concentrations under the assumption of charge neutrality at the interface. On the premise that the surface is (at least close to) electroneutral, we determine that ~ 0.35 Cl^- anions (and accordingly ~ 0.675 Ba^{2+} cations) are bound per PG at 20 mN/m; these numbers decrease to ~ 0.15 Cl^- (~ 0.575 Ba^{2+}) at high pressure. Up to 45 mN/m, the highest pressure value we have studied, stoichiometric Ba^{2+} binding ($\text{Ba}^{2+}:\text{PG}^- = 0.5$) was never observed. In the case of DMPA monolayers on BaCl_2 we observed generally the same behavior of the subphase-borne anions; however, in that case we concluded that at high pressure ($\pi = 50$ mN/m) a stoichiometric ($\text{Ba}^{2+}:\text{PA}^- = 0.5$) ratio was obtained. We thus expect that the same stoichiometry should be observed for PG at even larger lateral pressures.

The half width of the distribution of the phosphate moiety along the surface normal σ_{int} does not change significantly along the isotherm. $\sigma_{\text{int}} = 2.0 \pm 0.1$ Å for all investigated pressures is $\sim 0.3, \dots, 0.5$ Å larger than the values observed with PA monolayers under similar preparation conditions.²⁸

The instrumentation described here brings the resolution of laboratory scale x-ray reflectivity measurements of planar organic surface films to a level that was until recently reserved for experiments at synchrotron facilities. Limitations in the available momentum transfer range that have so far confined the characterization of lipid surface film structure to the discussion of gross properties of the chain and the headgroup layers are thus overcome, and details of the lipid headgroups are becoming accessible. This is currently exploited by addressing such diverse issues as biomembrane structure in general,²⁸ the binding of peripheral proteins to membrane surfaces,^{20,21} the interaction of pharmaceuticals with membranes,⁴⁹ the electrostatics of charged interfaces, or the physics of polymer brushes.⁵⁰

Note Added in Proof: We have recently performed such a contrast variation experiment on a DMPA monolayer on a BaCl_2 -containing subphase by utilizing the anomalous scattering of Ba^{2+} ions in reflectivity measurements at various x-ray wavelengths at the 6-ID beamline of APS (Argonne, IL).

ACKNOWLEDGMENTS

This instrument has been cofinanced by the State of Saxony and the German Federation through the HBMG program (Project No. 3772-036-189). Bernd Kohlstrunk has designed and constructed the peripheral controllers (film balance control and Peltier power supply). The authors thank Kristian Kjaer who has constructed and maintained the BW1 reflectometer at HASYLAB for years and Markus Weygand for administration of the master computer system and assistance with the BW1 measurements. The experimental work has been supported by the Deutsche Forschungsgemeinschaft through Grant No. SFB 294 (TP F3) and the Fonds der Che-

mische Industrie, Frankfurt/M. We are also grateful to HASYLAB at DESY for BW1 beamtime under Contract No. II-99-078.

- ¹M. Lösche, E. Sackmann, and H. Möhwald, *Ber. Bunsenges. Phys. Chem.* **87**, 848 (1983).
- ²M. Lösche and H. Möhwald, *Rev. Sci. Instrum.* **55**, 1968 (1984).
- ³P. Krüger and M. Lösche, *Phys. Rev. E* **62**, 7031 (2000).
- ⁴S. Hénon and J. Meunier, *Rev. Sci. Instrum.* **62**, 936 (1991).
- ⁵D. Hönig and D. Möbius, *J. Phys. Chem.* **95**, 4590 (1991).
- ⁶M. Lösche, J. P. Rabe, A. Fischer, B. U. Rucha, W. Knoll, and H. Möhwald, *Thin Solid Films* **117**, 269 (1984).
- ⁷R. Reiter, H. Motschmann, H. Orendi, A. Nemetz, and W. Knoll, *Langmuir* **8**, 1784 (1992).
- ⁸J. Spinke, M. Liley, H.-J. Guder, L. Angermaier, and W. Knoll, *Langmuir* **9**, 1821 (1993).
- ⁹W. Knoll, M. R. Philpott, J. D. Swalen, and A. Giraldo, *J. Chem. Phys.* **77**, 2254 (1982).
- ¹⁰A. Nemetz, T. M. Fischer, A. Ulman, and W. Knoll, *J. Chem. Phys.* **98**, 5912 (1992).
- ¹¹R. A. Dluhy and D. G. Cornell, *J. Phys. Chem.* **89**, 3195 (1985).
- ¹²R. Mendelsohn, J. W. Brauner, and A. Gericke, *Annu. Rev. Phys. Chem.* **46**, 305 (1995).
- ¹³M. Weck, R. Fink, and H. Ringsdorf, *Langmuir* **13**, 3515 (1997).
- ¹⁴J. Als-Nielsen and K. Kjaer, in *Phase Transitions in Soft Condensed Matter*, edited by T. Riste and D. Sherrington (Plenum, New York, 1989), p. 113.
- ¹⁵J. Als-Nielsen and H. Möhwald, in *Handbook on Synchrotron Radiation*, edited by S. Ebashi, M. Koch, and E. Rubinstein (Elsevier, North-Holland, Amsterdam, 1991), p. 1.
- ¹⁶J. Als-Nielsen, D. Jacquemain, K. Kjaer, M. Lahav, F. Leveiller, and L. Leiserowitz, *Phys. Rep.* **246**, 251 (1994).
- ¹⁷K. Kjaer, J. Als-Nielsen, C. A. Helm, L. A. Laxhuber, and H. Möhwald, *Phys. Rev. Lett.* **58**, 2224 (1987).
- ¹⁸P. Dutta, J. B. Peng, B. Lin, J. B. Ketterson, M. Prakash, P. Georgopoulos, and S. Ehrlich, *Phys. Rev. Lett.* **58**, 2228 (1987).
- ¹⁹S. A. W. Verclas, P. B. Howes, K. Kjaer, A. Wurlitzer, M. Weygand, G. Büldt, N. A. Dencher, and M. Lösche, *J. Mol. Biol.* **287**, 837 (1999).
- ²⁰M. Weygand, B. Wetzler, D. Pum, U. B. Sleytr, K. Kjaer, P. B. Howes, and M. Lösche, *Biophys. J.* **76**, 458 (1999).
- ²¹M. Weygand, M. Schalke, P. B. Howes, K. Kjaer, J. Friedmann, B. Wetzler, D. Pum, U. B. Sleytr, and M. Lösche, *J. Mater. Chem.* **10**, 141 (2000).
- ²²J. Penfold and R. K. Thomas, *J. Phys.: Condens. Matter* **2**, 1369 (1990).
- ²³D. Vaknin, K. Kjaer, J. Als-Nielsen, and M. Lösche, *Biophys. J.* **59**, 1325 (1991).
- ²⁴H. Baltes, M. Schwendler, C. A. Helm, and H. Möhwald, *J. Colloid Interface Sci.* **178**, 135 (1996).
- ²⁵H. Yamaoka, H. Matsuoka, K. Kago, H. Endo, J. Eckelt, and R. Yoshitome, *Chem. Phys. Lett.* **295**, 245 (1998).
- ²⁶C. A. Helm, H. Möhwald, K. Kjaer, and J. Als-Nielsen, *Europhys. Lett.* **4**, 697 (1987).
- ²⁷C. A. Helm, P. Tippmann-Krayer, H. Möhwald, J. Als-Nielsen, and K. Kjaer, *Biophys. J.* **60**, 1457 (1991).
- ²⁸M. Schalke and M. Lösche, *Biochim. Biophys. Acta* (in press).
- ²⁹R. Frahm, J. Weigelt, G. Meyer, and G. Materlik, *Rev. Sci. Instrum.* **66**, 1677 (1995).
- ³⁰Four different stacks consisting of 1, 2, 4, and 8 Cu foils (thickness, ~ 35 μm each) provide the possibility to attenuate the beam in $2^4 = 16$ combinations. The resulting attenuation steps are equidistantly distributed on a logarithmic scale and separated from each other by a factor of ~ 2.6 .
- ³¹M. Lösche, M. Piepenstock, A. Diederich, T. Grünwald, K. Kjaer, and D. Vaknin, *Biophys. J.* **65**, 2160 (1993).
- ³²This limit is effectively reached as the numbers n and n_0 of background counts and signal counts get so close to each other even after extended count times, that the error bars $\Delta R = \sqrt{2R}/\sqrt{n}$ are infinitely long in the negative direction from R on the logarithmic scale.
- ³³K. Kjaer, J. Als-Nielsen, C. A. Helm, P. Tippmann-Krayer, and H. Möhwald, *J. Phys. Chem.* **93**, 3200 (1989).
- ³⁴P. S. Pershan, *Faraday Discuss. Chem. Soc.* **89**, 231 (1990).
- ³⁵P. S. Pershan, *Colloids Surf., A* **171**, 149 (2000).
- ³⁶J. Skov Pedersen, *J. Appl. Crystallogr.* **25**, 129 (1992).
- ³⁷J. Skov Pedersen and I. W. Hamley, *Physica B* **198**, 16 (1994).

- ³⁸X.-L. Zhou and S.-H. Chen, *Phys. Rev. E* **47**, 3174 (1993).
- ³⁹N. F. Berk and C. F. Majkrzak, *Phys. Rev. B* **51**, 11296 (1995).
- ⁴⁰C.-H. Chou, M. J. Regan, P. S. Pershan, and X.-L. Zhou, *Phys. Rev. E* **55**, 7212 (1997).
- ⁴¹M. C. Wiener and S. H. White, *Biophys. J.* **59**, 174 (1991).
- ⁴²H. I. Petrache, S. E. Feller, and J. F. Nagle, *Biophys. J.* **70**, 2237 (1997).
- ⁴³R. S. Armen, O. D. Uitto, and S. E. Feller, *Biophys. J.* **75**, 734 (1998).
- ⁴⁴M. C. Wiener and S. H. White, *Biophys. J.* **61**, 434 (1992).
- ⁴⁵M. Schalke, P. Krüger, M. Weygand, and M. Lösche, *Biochim. Biophys. Acta* **1464**, 113 (2000).
- ⁴⁶M. Schalke, Ph.D. thesis, Leipzig University, 2000.
- ⁴⁷While this is certainly an oversimplification, since the surface remains presumably net negatively charged, there is no means of determining the absolute concentration of both headgroup-bound cations or anions independent of each other at the present stage.
- ⁴⁸V. M. Kaganer, H. Möhwald, and P. Dutta, *Rev. Mod. Phys.* **71**, 779 (1999).
- ⁴⁹W. Caetano, M. Ferreira, M. Tabak, M. I. Mosquera Sanchez, O. N. Oliveira Jr., P. Krüger, M. Schalke, and M. Lösche, *Biophys. Chem.* (submitted).
- ⁵⁰A. Wurlitzer *et al.*, *Macromolecules* (submitted).